KOH assistance with graphene oxide induced synthesis of porous carbon nanosheets for supercapacitor and zinc ion hybrid capacitor

Lan Wang [a, ‡, *], Shuya Zhang [b, ‡], Lingxuan Hu [a], Xiaoliang Wu [c, *] and Xiaobin Fan [b, *]

[a] *School of New Energy, Ningbo University of Technology, Ningbo 315336, Zhejiang, China*

[b] *State Key Laboratory of Chemical Engineering, Collaborative Innovation Center of Chemical Science and Engineering, School of Chemical Engineering and Technology, Tianjin University, Tianjin 300072, China*

[c] *College of Chemistry, Chemical Engineering and Resource Utilization, Northeast Forestry University, Harbin 150040, China*

‡ *These authors contributed equally to this work*

* *Corresponding Author*

E-mail: wanglan@nbut.edu.cn, wuxiaoliang90@163.com, xiaobinfan@tju.edu.cn

Supplementary Information

1.1 Materials

Potassium hydroxide (KOH), Sodium sulfate (Na_2SO_4), Zinc sulfate heptahydrate ($ZnSO_4 \cdot 7H_2O$), Hydrochloric acid (HCl), Polytetrafluoroethylene (PTFE) and ethanol were analytical-grade and obtained from Sinopharm Chemical Reagent, Co., Ltd (Shanghai, China). Zinc tablets (thickness 300 μm) were purchased from Guangdong Candlelight New Energy Technology Co., Ltd. and glass fiber diaphragm (GF/A) from Qingyuan Metal Materials Co.All raw materials were used directly as purchased without further purification. The water used in the experiments was freshly deionized.

1.2 Structural characterizations

The microstructures were measured by scanning/transmission electron microscope (SEM JEOL JSM-7500F, TEM JEM-2800F). Powder X-ray diffractometer (XRD) was used to characterize the crystal structures. X-ray photoelectron spectroscopy (XPS) measurement (Thermo Scientific K-Alpha) was used to detect the surface chemical state of the obtained samples. Nitrogen adsorption/desorption measurement was used to detect the specific surface area by the multi-point Brunauer-Emmett-Teller (BET) way and the pore size distribution was estimated by density functional theory (DFT).

1.3 Assembling symmetric supercapacitor

The electrochemical performance of the synthesized carbon materials was also evaluated in symmetrical device using two-electrode system in 1 M Na_2SO_4 solution. All measurements were tested by electrochemical workstation (CHI 660E).

1.4 Assembling Zinc-ion hybrid supercapacitor

The mass ratio contains 80 wt% hierarchical porous carbon, 10 wt% conductive carbon black and 5 wt% polytetrafluoroethylene (PTFE), and then mixed and ground with ethanol to form a uniform slurry with no particles on the surface. After coating on the stainless steel mesh with a coating thickness of approximately 150 μm, the loaded activated carbon is about 3 mg cm^{-2}. The electrode was vacuum dried overnight at 60 °C. To fabricate ZIHC, the prepared carbon electrode was used as the cathode, the zinc tablet was used as the anode, and the Wattman glass fiber was used as the separator. The aqueous 2 M $ZnSO_4$ was used as the electrolyte.

1.5 Electrochemical measurement

Electrochemical performance were studied using cyclic voltammetry (CV), galvanostatic charge-discharge (GCD) and electrochemical impedance spectroscopy (EIS) on a CHI660E electrochemical workstation (Chenghua, Shanghai, China) at room temperature. The CV curves of SCs was performed at scan rates of 2-100 mV s^{-1} in the voltage range between 0 and 1.6 V. The CV curves of ZIHCs was performed at scan rates of 2-100 mV s^{-1} in the voltage range between 0.2 and 1.8 V. GCD curves were tested at current densities ranging from 0.1 A g^{-1} to 10 A g^{-1}. EIS measurement was measured with a frequency range of 10^{-2} to 10^{5} Hz.

The gravimetric specific capacitance (C) was computed by the formulas:

$$C = \frac{I \times \Delta t}{m \times \Delta V} \quad (1)$$

where I is the current density, Δt is discharge time, ΔV is the potential region.

$$C = \frac{\int IdV}{vmV} \quad (2)$$

where I is the current density, V is potential region, v is the scan rate, and m is the mass of active materials.

The energy density and the power density of the devices are calculated according to equation (3) and (4), respectively:

$$E = \frac{C \times (\Delta V)^2}{2 \times 3.6} \quad (3)$$

$$P = \frac{3600 \times E}{\Delta t} \quad (4)$$

Where E (Wh kg^{-1}) is the energy density, P (W kg^{-1}) is the power density, C (F g^{-1}) is the specific capacitance of the SCs or ZIHCs, ΔV (V) is the operating voltage window of the SCs or ZIHCs, and Δt (s) is the discharge time.

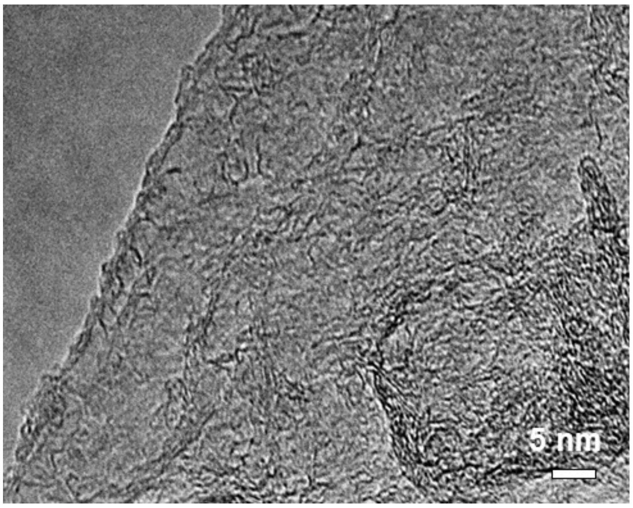

Fig. S1. High magnification TEM image of GPC-700.

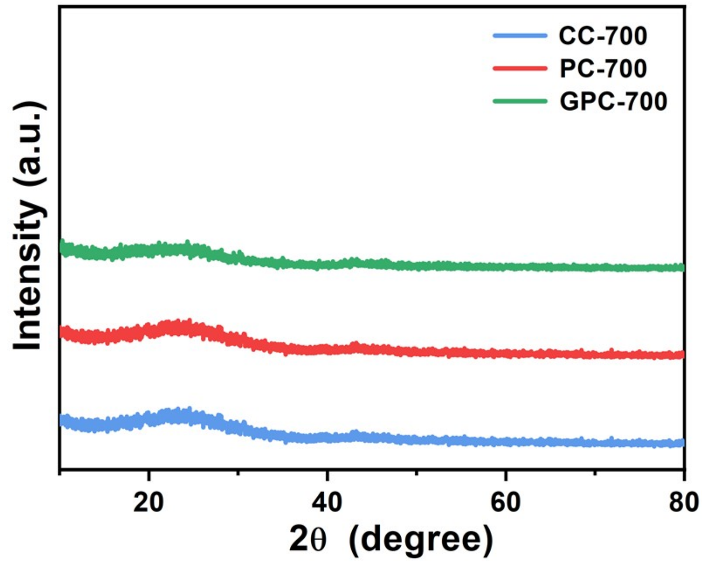

Fig. S2. XRD patterns of CC-700, PC-700 and GPC-700.

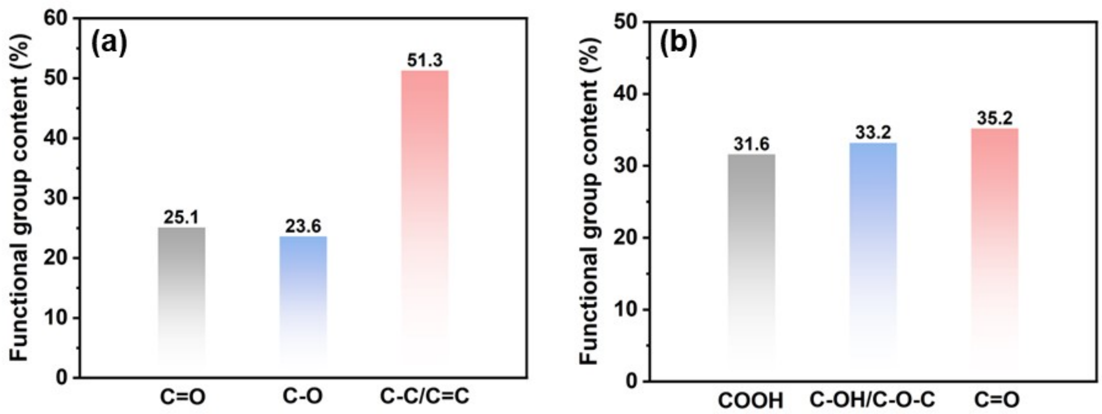

Fig. S3. (a) The percentage of each functional group in the high-resolution C 1s spectra. (b) The percentage of each functional group in the high-resolution O 1s spectra.

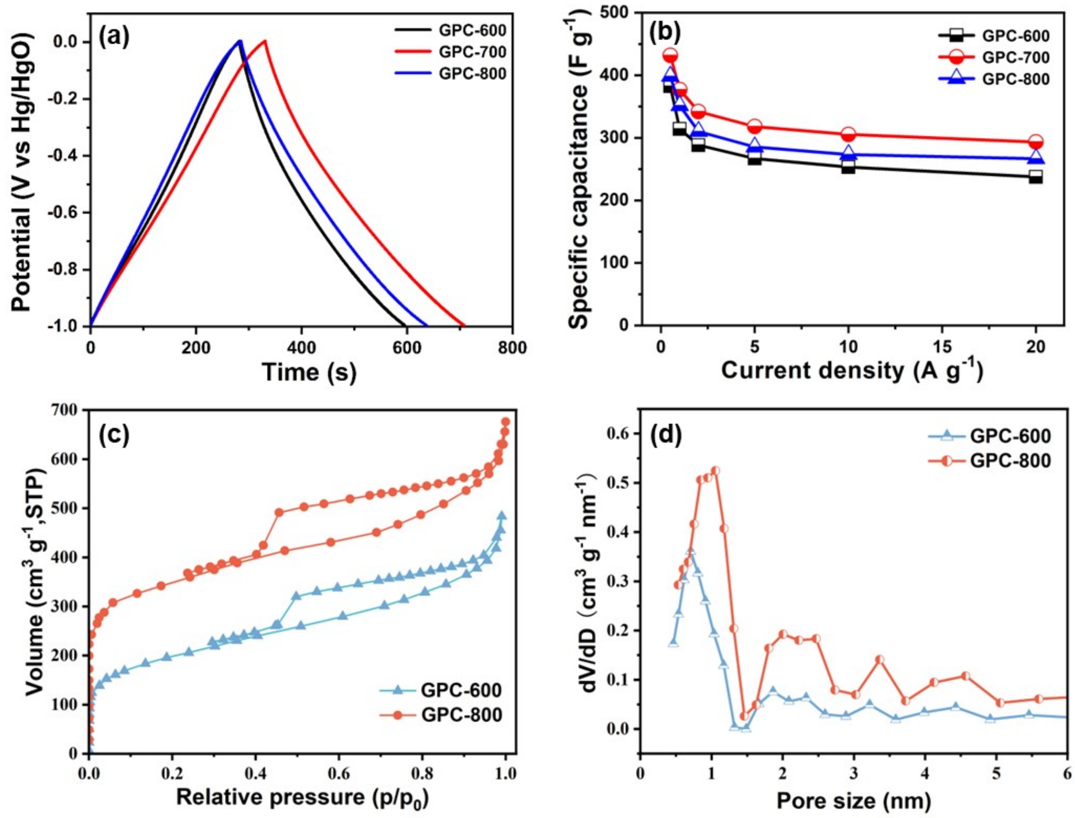

Fig. S4. (a) GCD curves of the GPC-600, GPC-700 and GPC-800 electrodes at 1 A g^{-1}. (b) Specific capacitance of the GPC-600, GPC-700 and GPC-800 electrodes at various current densities. (c) N_2 adsorption/desorption isotherms of GPC-600 and GPC-800. (d) Pore size distribution curve

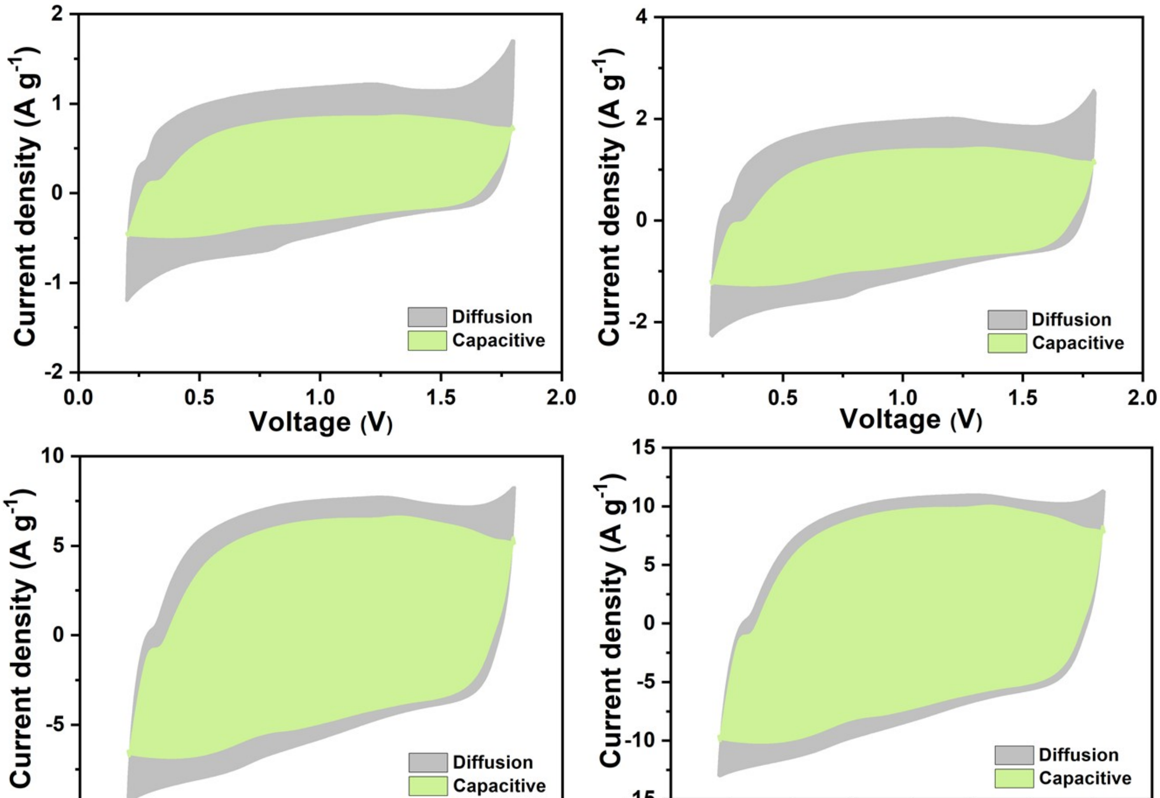

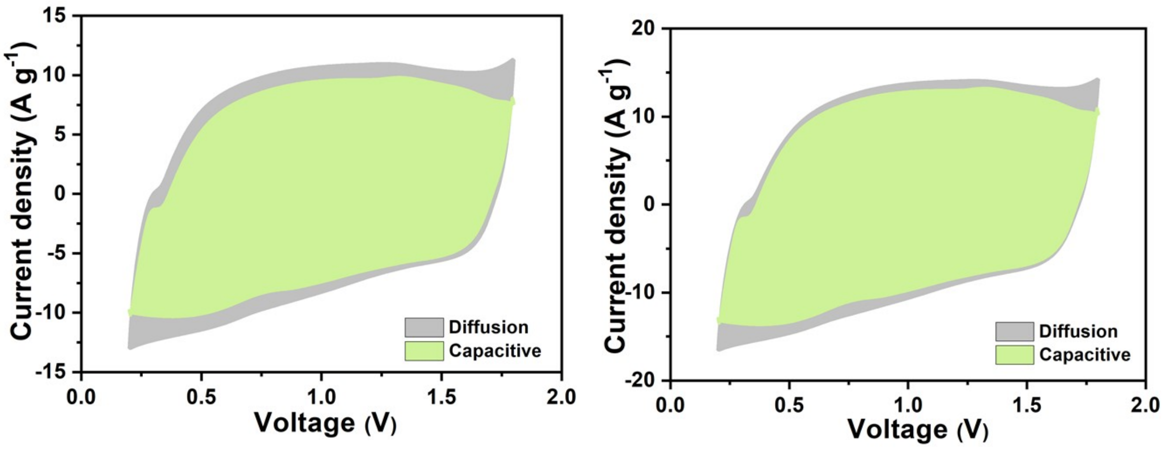

Fig. S5. Capacitance and diffusion-controlled contribution of Zn//$ZnSO_4$//GPC-700 ZIHC at different scanning rates.

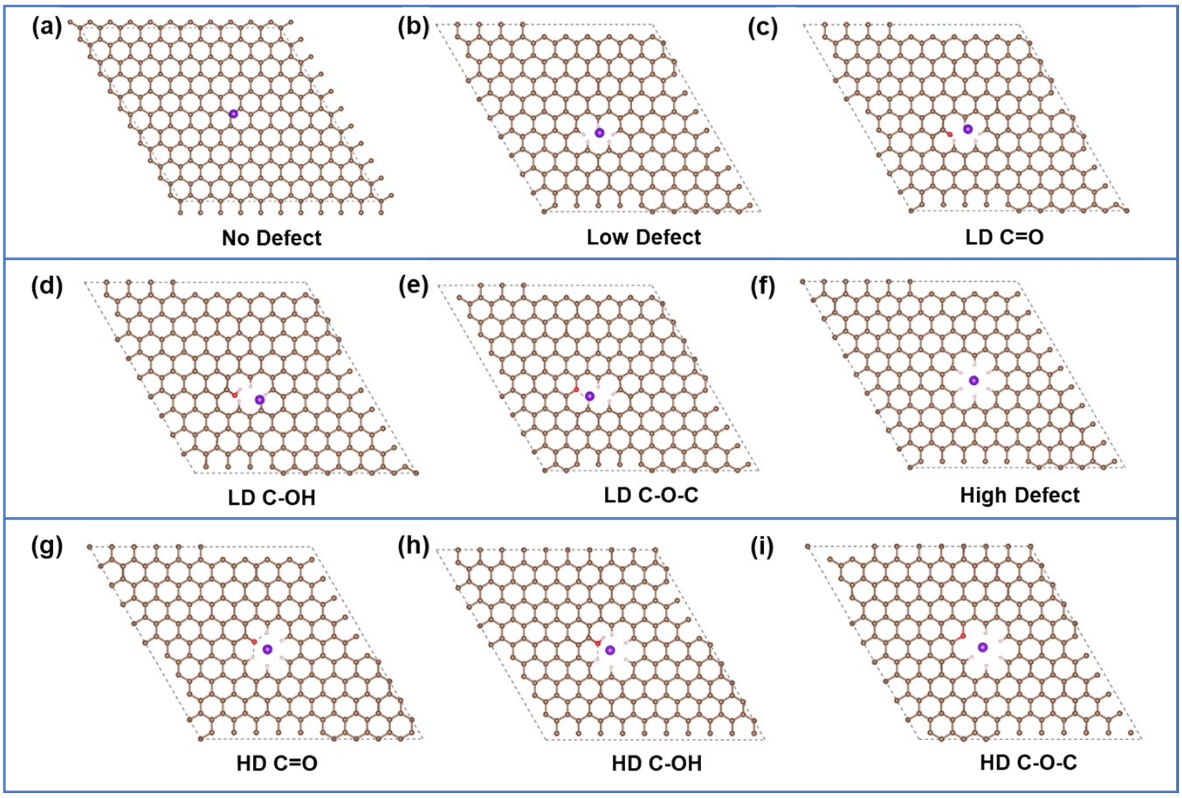

Fig. S6. First-principles calculations for Zn^{2+} storage behavior: Zn^{2+} was absorbed in the (a) No

Defect; (b) Low Defect; (c) LD C=O; (d) LD C-OH; (e) LD C-O-C; (f) High Defect; (g) HD C=O; (h) HD C-OH; (i) HD C-O-C.

Table S1 Performance comparison of GPC-700 with other porous carbons reported in literatures.

Samples	Electrolyte	Current density ($A\ g^{-1}$)	Specific capacitance ($F\ g^{-1}$)	Current density ($A\ g^{-1}$)	Specific capacitance ($F\ g^{-1}$)	Ref.
GPC-700	**6 M KOH**	**0.5**	**431.8**	**20**	**293.3**	**This work**
ZGCA-700	6 M KOH	0.5	284.7	50	170.1	[1]
p-RGO	3 M KOH	0.5	215.4	15	162	[2]
N3OPC-3	6 M KOH	0.5	463	10	335	[3]
NS-IPCN800	6 M KOH	0.05	302	40	231	[4]
GGI	6 M KOH	0.5	341	50	150	[5]
SNPCNS	6 M KOH	0.5	286	20	174.5	[6]

NOPC–KCa	6 M KOH	0.5	295.5	20	248.1	[7]
OHPC-1	6 M KOH	0.5	283	20	151	[8]
HPC-3	6 M KOH	0.5	287	50	172.2	[9]
CHPC	6 M KOH	0.5	328	20	230	[10]
AC-20	6 M KOH	0.5	309	20	198	[11]
NP-HPC$_2$	6 M KOH	0.05	309	50	211	[12]
WTCS	6 M KOH	0.1	339	20	258	[13]
NHPC-750-3	6 M KOH	0.5	310.1	20	238.7	[14]
OTS350-PC	6 M KOH	0.5	298	20	238.4	[15]

Table S2 The electrochemical properties of Zn ‖ 2 M $ZnSO_4$ ‖ GPC-700 ZIHC compared with the reported ZIHCs.

Samples	**Electrolyte**	**Current density (A g^{-1})**	**Specific capacity (mA h g^{-1})**	**Energy density (Wh kg^{-1})**	**Ref.**
GPC-700	**2 M $ZnSO_4$**	**0.1**	**162.6**	**123.1**	**This work**
HPCS-900	2 M $ZnSO_4$	0.1	104.9	90.17	[16]
SA-3	2 M $ZnSO_4$	1	76.8	100	[17]
TPC-7	2 M $ZnSO_4$	0.1	134.1	102	[18]
LHPC	1 M $ZnSO_4$	0.1	128.5	63.5	[19]
SPCs-700	2 M $ZnSO_4$	0.2	86.7	78.4	[20]
NPFC$_{700}$	$Zn(CF_3SO_3)_2$	0.1	163.6	60.1	[21]
LDC	1 M $ZnSO_4$	0.5	127.7	97.6	[22]

MOF-PC	2 M $ZnSO_4$	0.05	50	58.1	[23]
N-OPCNF	2 M $ZnSO_4$	0.1	136	72.3	[24]
NAC	2 M $ZnSO_4$	0.1	98	82	[25]
AH-PCs	2 M $ZnSO_4$	0.1	170.2	137.61	[26]
JKPC-4	2 M $ZnSO_4$	0.1	225	154	[27]
CNF-Zn-800	2 M $ZnSO_4$	0.2	156	132.8	[28]

Reference

1 T. Huo, Y. Wang, J. Wang, C. Chen, Y. Zhao, L. Guo and X. Wu, N, O co-doped porous carbon decorated on porous graphene for zinc ion hybrid capacitor, *Adv. Sustain. Syst.*, 2025, **9**, 2400807.

2 S. Han, L. Xu, Z. Wang, C. Liu, M. Fu and B. Yuan, A low-cost salt-tolerant solar evaporator prepared from graphite in spent LIBs for high efficiency seawater desalination, *Chem. Eng. J.*, 2024, **498**, 154852.

3 G. Cui, Y. Guan, N. Huang, Y. Zhao and H. Wang, N, O-codoped porous carbon derived from longan shells for high-performance supercapacitor electrodes, *ACS Appl. Energy Mater.*, 2025, **8**, 7002-7012.

4 Y. Wei, J. Zhou, L. Yang, J. Gu, Z. Chen and X. He, N/S co-doped interconnected porous carbon nanosheets as high-performance supercapacitor electrode materials, *New Carbon Mater.*, 2022, **37**, 707-715.

5 Y. Yan, X. Hao, L. Gao, S. Lin, N. Cui, Y. Li, C. Hao, T. Ma and H. Wang, Highly accessible hierarchical porous carbon from a bi-functional ionic liquid bulky gel: high-performance electrochemical double layer capacitors, *J. Mater. Chem. A*, 2019, **7**, 25297-25304.

6 C. Chen, M. Zhao, Y. Cai, G. Zhao, Y. Xie, L. Zhang, G. Zhu and L. Pan, Scalable synthesis of strutted nitrogen doped hierarchical porous carbon nanosheets for supercapacitors with both high gravimetric and volumetric performances, *Carbon*, 2021, **179**, 458-468.

7 Y. Sun, Z. Sheng, E. Chen, Z. Tang, J. Wang, X. Zhu, Z. Wang, X. Li, X. Xie and X. Lin, Tuning the pore structure of N/O co-doped porous carbon nanosheets for high-performance supercapacitors and zinc-ion capacitors, *Int. J. Hydrogen Energy*, 2025, **118**, 35-45.

8 H. Liu, Y. Wang, L. Lv, X. Liu, Z. Wang and J. Liu, Oxygen-enriched hierarchical porous carbons derived from lignite for high-performance supercapacitors, *Energy*, 2023, **269**, 126707.

9 Y. Zhu, Z. Li, Y. Tao, J. Zhou and H. Zhang, Hierarchical porous carbon materials produced from heavy bio-oil for high-performance supercapacitor electrodes, *J. Energy Storage*, 2022, **47**, 103624.

10 D. Dong, Y. Zhang, Y. Xiao, T. Wang, J. Wang and W. Gao, Mechanochemistry coupled with $MgCO_3$ one-step activation to prepare coal-based hierarchical porous carbon for supercapacitors, *J. Power Sources*, 2021, **503**, 230049.

11 D. Dong, Y. Zhang, Y. Xiao, T. Wang, J. Wang and W. Pan, Synthesis of O-doped coal-based carbon electrode materials by ultrasound-assisted bimetallic activation for application in supercapacitors, *Appl. Surf. Sci.*, 2020, **529**, 147074.

12 H. Bi, X. He, H. Zhang, H. Li, N. Xiao and J. Qiu, N, P co-doped hierarchical porous carbon from rapeseed cake with enhanced supercapacitance, *Renew. Energ.*, 2021, **170**, 188-196.

13 J. Wu, M. Xia, X. Zhang, Y. Chen, F. Sun, X. Wang, H. Yang and H. Chen, Hierarchical porous carbon derived from wood tar using crab as the template: Performance on supercapacitor, *J. Power Sources*, 2020, **455**, 227982.

14 X. Wu, J. Liu, Y. Wang, Y. Zhao, G. Li and G. Zhang, Fabrication of porous carbon nanosheets via urea-promoted activation of potassium citrate for enhanced supercapacitor performance, *Chem. Eng. J.*, 2025, **512**, 162487.

15 X. Yang, S. Zhao, Z. Zhang, Y. Chi, C. Yang, C. Wang, Y. Zhen, D. Wang, F. Fu and R. Chi, Pore structure regulation of hierarchical porous carbon derived from coal tar pitch via pre-oxidation strategy for high-performance supercapacitor, *J. Colloid Interface Sci.*, 2022, **614**, 298-309.

16 K. Shang, Y. Liu, P. Cai, K. Li and Z. Wen, N, P, and S co-doped 3D porous carbon-architectured cathode for high-performance Zn-ion hybrid capacitors, *J. Mater. Chem. A*, 2022, **10**, 6489-6498.

17 X. Pan, Q. Li, T. Wang, T. Shu and Y. Tao, Controllable synthesis of electric double-layer capacitance and pseudocapacitance coupled porous carbon cathode material for zinc-ion hybrid capacitors, *Nanoscale*, 2024, **16**, 3701-3713.

18 Y. Liu, A. Liu, W. Song, H. Peng, M. Li, R. Yang and F. Wang, Triphenylene-derived oxygen-enriched hierarchical porous carbon nanosheets: Carbonization mechanism and application in zinc-ion hybrid capacitors, *J. Power Sources*, 2024, **603**, 234484.

19 J. Ma, S. Yang, T. Huang, X. Zu, Y. Sun and W. Zhang, 3D hierarchical tri-doped porous carbon derived from calcium lignosulfonate for high-performance zinc ion hybrid

capacitors, *New J. Chem.*, 2023, **47**, 17549-17557.

20 L. Liu, Y. Lu, D. Qiu, D. Wang, Y. Ding, G. Wang, Z. Liang, Z. Shen, A. Li, X. Chen and H. Song, Sodium alginate-derived porous carbon: Self-template carbonization mechanism and application in capacitive energy storage, *J. Colloid Interface Sci.*, 2022, **620**, 284-292.

21 F. Wei, Y. Wei, J. Wang, M. Han and Y. Lv, N, P dual doped foamy-like carbons with abundant defect sites for zinc ion hybrid capacitors, *Chem. Eng. J.*, 2022, **450**, 137919.

22 Y. Lu, Z. Li, Z. Bai, H. Mi, C. Ji, H. Pang, C. Yu and J. Qiu, High energy-power Zn-ion hybrid supercapacitors enabled by layered B/N co-doped carbon cathode, *Nano Energy*, 2019, **66**, 104132.

23 X. Qiu, N. Wang, Z. Wang, F. Wang and Y. Wang, Towards high-performance zinc-based hybrid supercapacitors via macropores-based charge storage in organic electrolytes, *Angew. Chem. Int. Ed.*, 2021, **60**, 9610-9617.

24 H. He, J. Lian, C. Chen, Q. Xiong, C. C. Li and M. Zhang, Enabling multi-chemisorption sites on carbon nanofibers cathodes by an in-situ exfoliation strategy for high-performance Zn–ion hybrid capacitors, *Nano-Micro Lett.*, 2022, **14**, 106.

25 N. Chang, T. Li, R. Li, S. Wang, Y. Yin, H. Zhang and X. Li, An aqueous hybrid electrolyte for low-temperature zinc-based energy storage devices, *Energy Environ. Sci.*, 2020, **13**, 3527-3535.

26 G. Chen, S. Chen, X. Wu, C. Wu, Y. Xiao, H. Dong, X. Yu, Y. Liang, H. Hu and M. Zheng, Ammonium persulfate assisted synthesis of ant-nest-like hierarchical porous carbons derived from chitosan for high-performance supercapacitors and zinc-ion hybrid capacitors, *J. Mater. Chem. A*, 2024, **12**, 11920-11935.

27 Q. Chu, Z. Chen, C. Cui, C. Xie, Z. Wei, X. Li, Y. Xu, Y. Li, Y. Cui and S. Pei, Jackfruit waste derived oxygen-self-doped porous carbon for aqueous Zn-ion supercapacitors, *J. Power Sources*, 2025, **629**, 235931.

28 G. Yang, Q. Zhang, C. He, Z. Gong, Z. Liu, J. Song, S. Jiang, J. Han, H. Yang, X. Li, Z. Pei and S. He, Bionic hollow porous carbon nanofibers for energy-dense and rapid zinc ion storage, *Angew. Chem. Int. Ed.*, 2025, **64**, e202421230.